Biochimica et Biophysica Acta, 704 (1982) 75–89
Elsevier Biomedical Press

BBA 31139

AN EXAMINATION OF THE CYANIDE DERIVATIVE OF BOVINE SUPEROXIDE DISMUTASE WITH ELECTRON-NUCLEAR DOUBLE RESONANCE

HARLAN L. VAN CAMP *, RICHARD H. SANDS [a] and JAMES A. FEE [b,**]

[a] *Department of Physics and* [b] *Department of Biological Chemistry, Biophysics Research Division, Institute of Science and Technology, The University of Michigan, Ann Arbor, MI 48109 (U.S.A.)*

(Received October 23rd, 1981)

Key words: Superoxide dismutase; Electron-nuclear double resonance; Cyanide derivative; (Bovine)

The Cu(II) sites of native, azido- and cyano-derivatives of bovine superoxide dismutase (superoxide:superoxide oxidoreductase, EC 1.15.1.1) have been examined by electron-nuclear double resonance (ENDOR). The ENDOR spectrum of the native protein taken at the $g_{\|}$ extreme shows resolved structure due to the directly coordinated N-atoms of the histidine ligands. These spectra are too complex for interpretation but suggest inequivalent coupling between the electronic spin and the four ligand N-atoms. By contrast, the azido protein reveals one type of nitrogen with well-resolved hyperfine and quadrupole splittings ($A_{zz} = 37.9 \pm 1$ MHz, $P_{zz} = 1.54 \pm 0.02$ MHz), and the cyano form reveals one well-resolved set of nitrogen lines ($A_{zz} = 47.8 \pm 0.4$ MHz, $P_{zz} = 1.62 \pm 0.01$ MHz) and one type of partially resolved nitrogen ($A_{zz} = 37.0 \pm 1$ MHz). The cyano form also reveals a complex spectrum in the low-frequency domain (1–10 MHz). Through isotopic substitution and computer simulation, the spectrum is shown to be a composite of the ENDOR from the remote imidazole nitrogens and the cyanide nitrogen. The component of the hyperfine constant perpendicular to the $C^{14}N$ bond axis is $A_{\perp}^{N} = 3.9 \pm 0.3$ MHz and along the bond axis is $A_{\perp}^{N} \cong 5.7$ MHz. The quadrupole interaction appears to be greatest along the CN axis with $Q_{z'z'} = 1.0 \pm 0.1$ MHz and $Q_{x'x'y'y'} \approx 0$. Based on an analysis of the hyperfine and quadrupole interactions seen at two extremes of the electron paramagnetic spectrum, we propose a square-planar arrangement of three imidazole nitrogen and one CN^- carbon around the copper. Within this plane two imidazole nitrogens are strongly coupled and magnetically equivalent, the third is inequivalent (slightly weaker hyperfine interaction) and forms a *trans* relationship with the cyanide. This model is consistent with other observations on the cyano-derivative.

Introduction

During the past several years considerable work has been done on the structure of the metal binding sites of bovine superoxide dismutase (superoxide:superoxide oxidoreductase, EC 1.15.1.1). This protein has a molecular weight of approx. 32000, has two identical polypeptide subunits each of which contains a copper and a zinc atom, and derives its most common name from its ability to catalyse the reaction $2\,O_2^- + 2\,H^+ \rightarrow H_2O_2 + O_2$. X-ray diffraction studies [1–3] on crystalline protein have revealed a copper binding site in which four imidazoles (belonging to histidines-44, 46, 61 and 118) coordinate to the Cu(II). One of the histidines (His-61) contributes an imidazolate bridge between the copper and the zinc. Although

* Present address: Biomedical Physics Division, Cancer Research and Treatment Center, University of New Mexico, Albuquerque, NM 87131, U.S.A.

** To whom correspondence should be addressed at: Biophysics Research Division, 2200 Bonisteel Blvd., Ann Arbor, MI 48109, U.S.A.

Abbreviations: EPR, electron paramagnetic resonance; ENDOR, electron-nuclear double resonance; ESE, electron spin echo; *S/N*, signal-to-noise ratio; RF, radio frequency; p-p, peak-to-peak.

one coordination site is shielded from the solvent by the protein body, a fifth site appears to be available for ligation of certain solutes, and it has been emphasized [4] that an 'open' coordination site is necessary for catalysis. The relevance of this site to the dismutation process is supported by the observation that known ligands of Cu(II), such as cyanide (CN^-) and azide (N_3^-) anions, are inhibitors [5] of catalysis.

Gaber et al. [6] have used NMR relaxivity of the Cu(II) to show that water is bound to the metal in the native protein and that CN^- probably displaces the water [7]. Moreover, the electron paramagnetic resonance (EPR) spectrum of holoprotein changes markedly on binding CN^-, and the resulting spectrum reveals the presence of three nearly equivalent nitrogens in the copper hyperfine spectrum [7–11]. Rotilio et al. [8] and Haffner and Coleman [12] showed, using $^{13}CN^-$, that the cyanide binds to the copper via its carbon atom. Lieberman et al. [13] have recently described cyanide-induced changes in the *g*-tensor principal axis system as seen through the EPR of crystalline dismutase, and cyanide has been shown to induce changes in the electronic structure of the remote imidazole nitrogen as observed [14] by the electron spin echo effect (ESE).

While structural studies of the native protein by X-ray diffraction clearly show that four nitrogens are bound to the copper [1–3], the EPR spectrum of the cyano complex is only consistent with there being three atoms magnetically coupled to the Cu(II). Further, even though a fifth coordination site is available at the copper, it is not clear how the active site is changed after the binding of an inhibitor (CN^-, N_3^-).

This article describes the application of electron -nuclear double resonance (ENDOR) to the Cu(II) site of bovine dismutase. It presents observations of the hyperfine and quadrupole interactions between the unpaired electron of the Cu(II) and both the coordinated and remote N-atoms of the liganding imidazole rings and the cyanide nitrogen. Since the native protein did not yield interpretable spectra and the azido complex revealed only one magnetic class of coordinated nitrogen atoms, the bulk of this study deals with the monocyano complex. Our observations suggest that in this complex there are two magnetically equivalent imidazole N-atoms and a third imidazole N-atom having a distincly different hyperfine interaction with the Cu(II) electron. Evidence, based partially on computer simulations, will be presented which suggests that the cyano complex is a square-planar arrangement of $(His\text{-}N)_3$ Cu(II)-CN in which the two N atoms *cis* to the CN are magnetically equivalent and the *trans* N-atom has slightly different magnetic interactions with the Cu(II). The biochemical implications of this model will be discussed briefly.

Materials and Methods

Most of the sample preparation and experimental procedures for this work have been described elsewhere. Bovine superoxide dismutase was obtained from Diagnostic Data, Inc., Mountain View, CA. Apoprotein was made following procedures given by McCord and Fridovich [15] and Fee [16]. The apoprotein was reconstituted with ^{65}Cu and ^{67}Zn [9]. The monocyano complex was then formed following the procedure of Fee and Gaber [7]. Enriched $KC^{15}N$ was obtained from Stohler Chemicals, Waltham, MA. All ENDOR samples (vol.$\approx$ 1 ml) used in this study were 1–2 mM in copper, buffered with 0.5 M PO_4 at pH 7.4, contained 20–40% glycerol by volume, and were frozen in liquid nitrogen immediately after preparation.

The ENDOR spectrometer has also been described elsewhere [17,18], but we mention some features of it that are important for this work. The spectrometer employs field modulation at 100 kHz, homodyne detection, low-power radio frequency (RF) radiation (on the order of 1 Gauss at 10 MHz), and a microwave reference arm for discrimination between absorption and dispersion. Because the cavity end of the spectrometer resides in a liquid-helium cryostat, we were able to make long-term (several hours when needed) observations at stable temperatures of 2 k, 4.2 k and 77 K. All EPR spectra presented here will be in the absorption mode at a temperature of 77 K, but the ENDOR spectra will be presented in the dispersion mode at temperatures of 1.8–2 K.

The ENDOR technique is well known [19] for its ability to recover hyperfine and quadrupole information from incompletely resolved EPR spectra. To perform the experiment one holds the magnetic field, H_0, constant on a partially

saturated EPR line and applies a second, or double resonant radiation to the sample. The frequency of this second radiation depends, in part, on the expected energy-level splittings of the hidden hyperfine structure; in this work the frequency range will be from 1–35 MHz. The ENDOR response is observed as a change in the constantly monitored EPR signal. The unresolved hyperfine structure may be associated with the parent nucleus or, as in the pesent paper, with the nuclei of surrounding ligands. When the hyperfine interactions are anisotropic one can also hope to obtain valuable structural information from a study of the ENDOR response as a function of the orientation of the complex in the static magnetic field. In this work we perform such a study, but it is limited by the sample being a frozen solution. The EPR from a frozen solution will be a powder spectrum, i.e., a superposition of the EPR from the many 'frozen' orientations of the protein relative to the external magnetic field. Usually ENDOR taken from EPR powder spectra will also yield powder spectra. In some cases [20], however, it is possible to pick out from the random sample a subset of molecules that represents a given orientation or class of orientations. Each of these situations will be presented in the following observations and discussion.

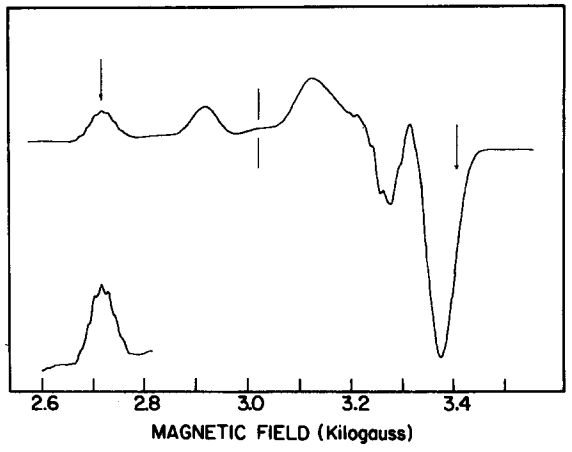

Fig. 1. Electron paramagnetic resonance spectrum of $^{65}Cu^{67}Zn$ bovine superoxide dismutase-$C^{15}N$. The sample was 0.88 mM in protein, buffered at pH 7.4 with 0.5 M PO_4, and had a volume of about 1 ml with 25% glycerol. The two arrows mark the field positions where ENDOR was performed. The $g_{\|}$ extreme is on the left, the $g_{\perp}$ extreme on the right. An enlargement of the low-field copper hyperfine peak shows superhyperfine structure characteristic of the three nearly equivalent nitrogens. Some instrumental conditions: microwave frequency = 9.334 GHz, power = 1 mW, field modulation amplitude = 4 $G_{p\text{-}p}$.

Results

The EPR spectrum of the monocyano derivative of $^{65}Cu^{67}Zn$-substituted superoxide dismutase is presented in Fig. 1. The rhombic spectrum of the native enzyme has been changed to an apparently axial one by the presence of the cyanide. Two of the ^{65}Cu hyperfine peaks are visible at the low-field portion of the spectrum, while the other two are somewhat less discernable at high field; we have marked the approximate position of $g_{\|} = 2.208$. The lowest-field ^{65}Cu hyperfine peak shows the ^{14}N superhyperfine structure characteristic of the three nearly equivalent nitrogens mentioned above, and some superhyperfine structure is also visible at the high-field end. We have indicated the field positions at which ENDOR was performed by the two arrows. An ENDOR experiment performed in the $g_{\|}$ extreme will be sensitive to only the subset of sample molecules having the static field, H_0, parallel to the $g_{\|}$ direction. Therefore, powder effects will be at a minimum. The experiment peformed at the high field ($g_{\perp}$ extreme) will, on the other hand, reflect all orientations for which H_0 is perpendicular to the $g_{\|}$ direction. Thus crystal-like ENDOR spectra can be expected at the $g_{\|}$ extreme, but powder ENDOR is expected at the $g_{\perp}$ extreme.

We divide our presentation of ENDOR spectra into high (10–35 MHz) and low (1–10 MHz) frequency regions because the high-frequency region is more intense than the low-frequency region, is best observed under particular instrumental conditions, and will be shown to represent a distinct set of nuclei. Fig. 2 shows spectra of the $C^{14}N^{-}$ annated protein taken at the $g_{\|}$ extreme in the high-frequency region. These traces were best obtained with a field modulation amplitude of 6 $G_{p\text{-}p}$ and with the aid of frequency modulation superimposed upon the radio frequency oscillation (modulation frequency = 1 kHz and frequency deviation = 150 kHz). We have reported [17] that the latter seems to improve the signal-to-noise ratio,

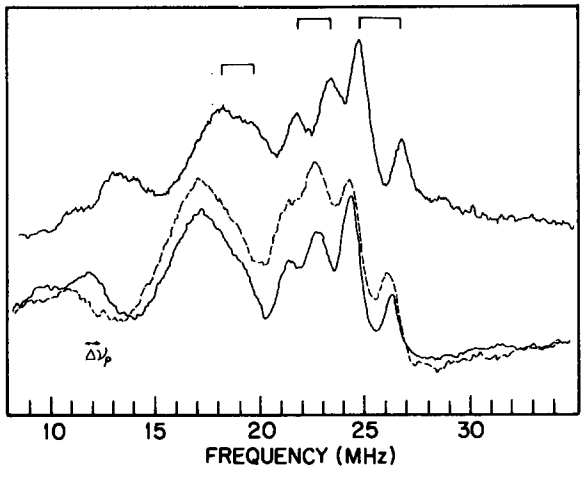

Fig. 2. ENDOR of bovine superoxide dismutase-$C^{14}N$ at the $g_{\|}$ extreme, high-frequency region. The radio frequency increased for the upper and decreased for the lower traces. The lower two traces (A, B) were taken at two separate microwave frequencies (9.056, 8.505 GHz). The expected shift in a proton resonance is shown by the arrow labeled $\Delta\nu_p$. Nuclear Zeeman pairs for ^{14}N are indicated for the two types of strongly coupled nitrogen. Experimental conditions: microwave power $\lesssim$0.1 mW, T=1.9 K, modulation amplitude=6 $G_{p\text{-}p}$, sweep rate=0.26 MHz/s, and accumulation time=40 min.

S/N, for these and other copper complexes even though no lock-in detection at this modulation frequency was used. The S/N improvement may be related to that also found from fast RF sweep times. The RF was swept upward (8 to 35 MHz) at a rate of 0.27 MHz/s for the upper trace in Fig. 2, but downward for the lower two traces. In each case we call attention to three regions. There are four relatively sharp bands centered around 23 MHz, a partially resolved band at 18 MHz, and a weaker band centered at about the free proton frequency (11.3 MHz). The experimental conditions and instrumental parameters corresponding to these spectra seem to enhance the S/N and clarity of the peaks above 18 MHz while suppressing the proton region (8–13 MHz). Other conditions will bring about the reverse situation, but we will not concentrate on the protons in this work.

There are some differences between the upper and lower traces in Fig. 2 that we attribute to relaxation and rapid passage effects. There is a small but noticeable shift between the upper and lower traces in the direction of the sweep. Because of this shift, the resonant frequencies of sharp features were determined by taking an average of traces swept alternately forward and backward. There are some slight differences in the lineshape between the upper and lower traces, notably at the 18 MHz band where a high-frequency shoulder is more prominant when the RF is swept upward. The two lower traces were obtained at the same g-value, but for different microwave frequencies. Comparing the two enables one to discriminate between resonances associated with protons and other nuclei [21], provided that these two nuclei have significantly different nuclear magnetic moments (see Discussion). The ENDOR in the high-frequency region was independent of whether we used $C^{15}N$ or $C^{14}N$. We also observed that when the ENDOR patterns were followed from the $g_{\|}$ to the $g_{\perp}$ extreme, the center of the cluster of four peaks near 23 MHz moved up to about 27.5 MHz, extended over a 6 MHz breadth and became less well-resolved. The feature at 18 MHz moved only slightly to higher frequency (data not presented).

The ENDOR spectra of native and azido proteins taken at the $g_{\|}$ extreme are shown in Fig. 3. The native protein (upper trace) shows an apparent triplet of lines centered around 18 MHz.

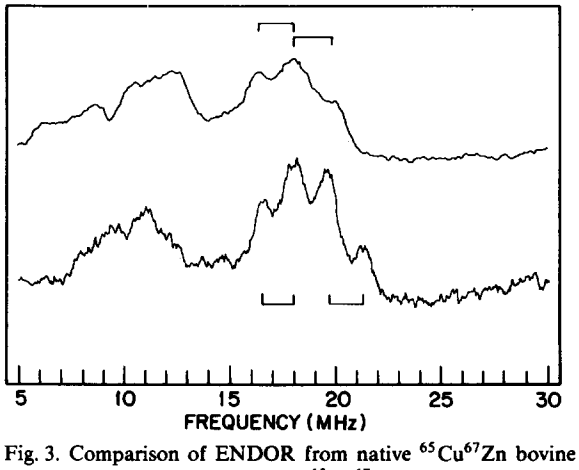

Fig. 3. Comparison of ENDOR from native $^{65}Cu^{67}Zn$ bovine superoxide dismutase (top) and $^{65}Cu^{67}Zn$ bovine superoxide dismutase-N_3^- (bottom) at the low-field extreme. The azido-bovine superoxide dismutase (1 mM in copper) was derived from this native bovine superoxide dismutase sample (2 mM in copper). Instrumental settings were approximately the same as in Fig. 2 except that the accumulation time of the lower trace was 3-times as long as the upper trace (i.e., 20 min). In both traces, the RF is decreasing.

When recorded at the high-field extreme, this triplet spreads out from 17 to 27 MHz, suggesting possible anisotropy and differences in the coupling constants of the individual N-atoms with the Cu(II). The spectrum of the azido ($^{14,14,14}N_3^-$) complex shows four peaks and is thus quite similar to the cyano complex. However, this pattern has a central frequency near 19 MHz, compared to 24 MHz for the cyano complex. It is noteworthy that neither the native protein nor the azido complex show resolved superhyperfine structure in their EPR spectra.

Of the three forms of protein studied here, the cyano form provided the most interesting spectra in the low frequency (1–10 MHz) region. These observations will now be presented. Each of Figs. 4–7 contains one or two ENDOR spectra taken under specific experimental conditions (solid lines). The different conditions concern the isotopic composition ($C^{15}N$ and $C^{14}N$), the static magnetic field value ($g_{\|}$ or $g_{\perp}$ extreme), and other instrumental settings. The experimental spectra are compared to computer-generated spectra (dashed lines) to be discussed later.

The effect of $C^{15}N$ at the $g_{\perp}$ extreme is presented by the upper and lower traces of Fig. 4. The two experimental traces, each showing two bands peaked at about 2 and 4 MHz, were taken under slightly different experimental conditions. The upper trace swept the RF upward at a rate of 0.45 MHz/s, while the lower trace swept the RF downward at a rate of 0.17 MHz/s. The accumulation time for each was about 0.5 h. One can see that each trace has its advantage; although the upper forward-swept trace has better S/N, the lower one has, perhaps, slightly better resolution in that a hint of structure appears in the high-frequency shoulder of the band near 4 MHz. The asymmetry of this band is more evident in the upper trace; a portion of the asymmetry may be related to the influence of the sweep rate on the rapid passage effects (see Fig. 5 of Ref. 19).

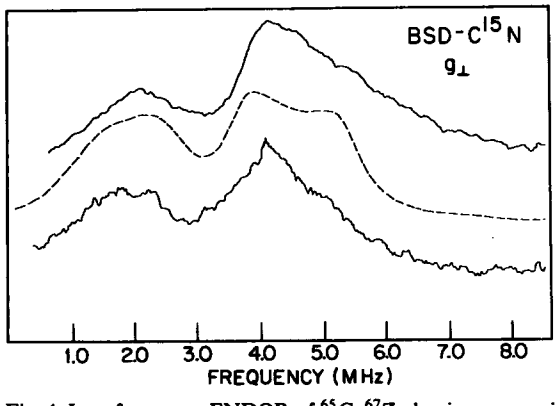

Fig. 4. Low-frequency ENDOR of $^{65}Cu^{67}Zn$ bovine superoxide dismutase-$C^{15}N$ at the $g_{\perp}$ extreme. The middle trace (dashed line) is a simulation described in the text and corresponds to parameters found in Table II. The upper and lower traces (solid lines) are both experimental, the upper being swept with increasing frequency at a rate of 0.44 MHz/s and the lower being swept with decreasing frequency at a rate of 0.17 MHz/s. The total accumulation time for each was about 0.5 h. Other conditions: microwave power = 0.1 mW, modulation amplitude = 2 $G_{p\text{-}p}$.

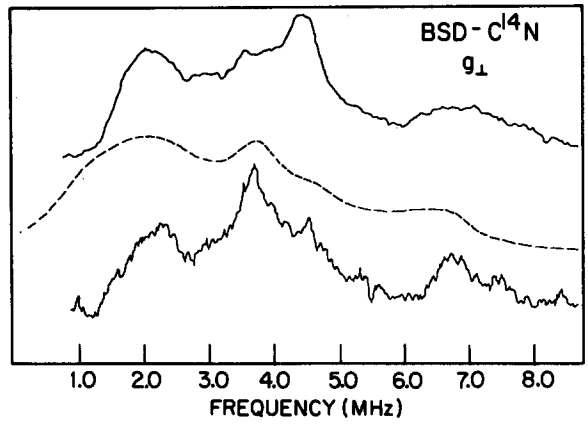

Fig. 5. Low-frequency ENDOR of $^{65}Cu^{67}Zn$ bovine superoxide dismutase-$C^{14}N$ at the $g_{\perp}$ extreme. The middle trace (dashed line) is a simulation described in the text and corresponds to parameters found in Table II. The upper and lower traces (solid lines) are experimental, the upper being swept with increasing frequency at a rate of 0.44 MHz/s and the lower with decreasing frequency at a rate of 0.17 MHz/s. The RF was frequency modulated at 1 kHz (frequency deviation, 150 kHz) for the upper but not for the lower trace. Total accumulation time was 1.6 h (upper trace) and 4.5 h (lower trace). Other instrumental settings were similar to Fig. 4.

In Fig. 5 we show the analogous spectra in the low-frequency region taken at the $g_{\perp}$ extreme of the $C^{14}N$ derivative. One immediately sees some differences between this and Fig. 4, especially near and above 4 MHz. We attribute these differences to the presence of the cyanide nitrogen. The experimental conditions for the upper traces in Figs. 4

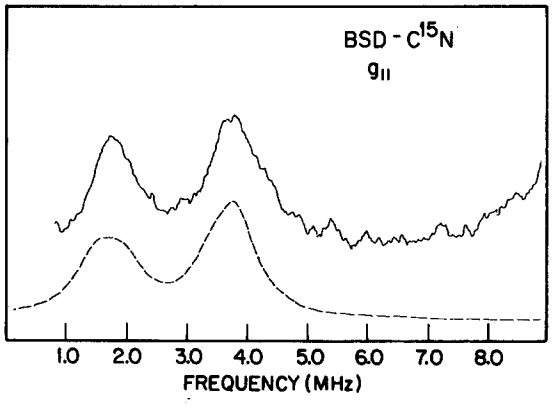

Fig. 6. Low-frequency ENDOR of $^{65}Cu^{67}Zn$ bovine superoxide dismutase-$C^{15}N$ at the $g_{\|}$ extreme. The upper trace (solid line) is experimental with instrumental conditions similar to the lower trace in Fig. 4. The edge of the proton ENDOR response can be seen near 9 MHz. The lower trace (dashed line) is a simulation (see text and Table II).

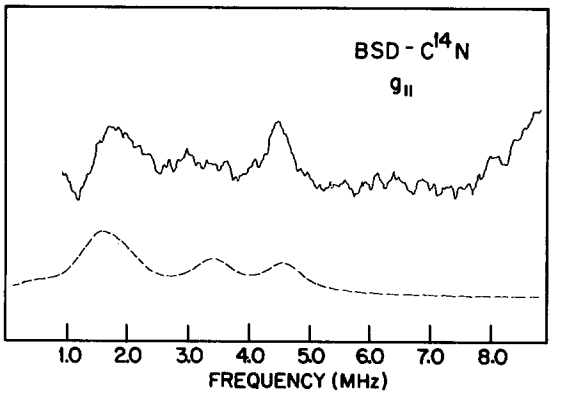

Fig. 7. Low-frequency ENDOR of $^{65}Cu^{67}Zn$ bovine superoxide dismutase-$C^{14}N$ at the $g_{\|}$ extreme. The upper trace (solid line) is experimental. Except for an accumulation time of about 1 h, the instrument settings were similar to those of the upper trace in Fig. 4.

and 5 are similar except that the total accumulation time of the latter was approx. 1.7 h (versus about 0.5 h for Fig. 4). Even through both samples were derived from equal portions of an original sample, the low-frequency spectrum for the $C^{14}N$ was weaker than that for the bovine superoxide dismutase-$C^{15}N$ derivatives. The RF, for the lower trace, was again swept downward at a rate of 0.17 MHz/s, but here we did not use small-amplitude (i.e., frequency deviation $<<$ ENDOR linewidths) superimposed frequency modulation. The resultant loss in the S/N demanded a longer accumulation time (4.5 h). Comparing the two experimental traces of Fig. 5, one can see that the experimental conditions not only affect the S/N, but also the lineshape. Most apparent is the intercharge of relative intensities of the peaks near 4 MHz. Nevertheless, these two traces are in qualitative agreement with regard to their major features, especially in the way the structure beyond 4 MHz differs from the $C^{15}N$ spectrum.

Figs. 6 and 7 compare the same ENDOR spectral region but taken at the $g_{\|}$ extreme. Again, the $C^{15}N$ sample was the more intense, having two strong lines for $C^{15}N$, but poor S/N allows us to identify only two bands at 2 and 4.5 MHz for the $C^{14}N$ derivative. The sweep-dependent shift that occurs in the high-frequency spectra of Fig. 2 is also present in Figs. 4–7. In each case the shift was no greater than 0.25 MHz, but because we will later compare Figs. 4–7 with simulated traces (the dashed lines), we have artificially shifted the experimental traces to the average position of the prominent features.

The spectra in the low-frequency region resemble those already reported [17] for the model compound, tetraimidazole-Cu(II). Since the analysis of the observations on the cyano complex will rely heavily on that already made for the model compound [17], we have reproduced in Fig. 8 its ENDOR spectrum taken at the $g_{\perp}$ extreme. As in the present case, the intensity in the low-frequency

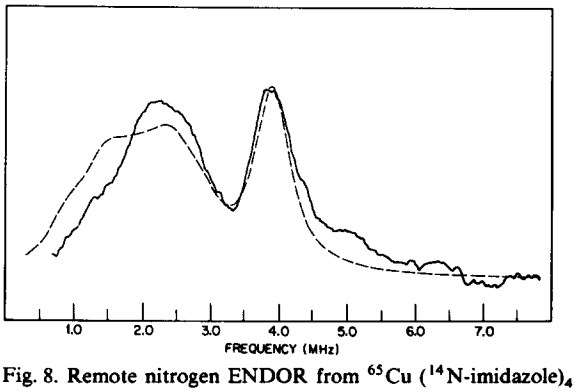

Fig. 8. Remote nitrogen ENDOR from ^{65}Cu (^{14}N-imidazole)$_4$ observed at the $g_{\|}$ extreme. Experimental (solid line), simulation (dashed line). See Ref. 17.

region was markedly reduced compared to the high frequency region, and the intensity in the low-frequency range was so low at the $g_{\|}$ extreme (where the EPR intensity is also low) that it discouraged study.

Discussion

High-frequency ENDOR

The cluster of four lines near 23.5 MHz in the ENDOR systems derived from $C^{14}N$ annated superoxide dismutase (Fig. 2) suggests one type of nitrogen. Such a four-line pattern is often seen in well-resolved ^{14}N spectra [22]. Under the assumption that the external and hyperfine fields point along the same direction as $g_{\|}$ we can write a first-order nuclear Hamiltonian for an electronic spin, S, interacting with a nuclear spin I, as

$$\mathcal{H}_N = A_{zz} S_z I_z + P_{zz}\left(I_z^2 - \frac{I(I+1)}{3}\right) - g_N \beta_N H_0 I_z \qquad (1)$$

where A_{zz} is the hyperfine constant observed at $g_{\|}$, and P_{zz} is the quadrupole constant observed along the static-field direction. We have assumed that the hyperfine and quadrupole terms have parallel principal axes. The last term is the nuclear Zeeman interaction defined by the nuclear g-factor, g_N, the nuclear magneton, β_N, and the static field, H_0. For a nuclear spin of $I = 1$, this Hamiltonian will lead to four hyperfine transitions given by:

$$\nu_{ENDOR} = \begin{cases} |A_{zz}/_2 + P_{zz} + g_N\beta_N H_0| & (2a) \\ |A_{zz}/_2 + P_{zz} - g_N\beta_N H_0| & (2b) \\ |A_{zz}/_2 - P_{zz} + g_N\beta_N H_0| & (2c) \\ |A_{zz}/_2 - P_{zz} - g_N\beta_N H_0| & (2d) \end{cases}$$

Eqn. 2a–d shows that the average of the four transitions will be determined by half the hyperfine constant, that pairs of lines occur separated by twice the nuclear Zeeman energy, and that the average position of these pairs will be separated by twice the quadrupole constant, P_{zz}.

The splitting of the nuclear Zeeman pairs is not only specific to a given isotope, but also is provided independently by the nuclear magnetic resonance technique. For a static field of $H_0 = 2600$ G we should expect $2 g_N \beta_N H_0 = 1.64$ MHz for ^{14}N. The Hamiltonian constants along with expected frequencies and splittings that were derived from a close inspection of the four-line patterns from the

TABLE I

CONSTANTS AND FREQUENCIES FOR STRONGLY COUPLED NITROGENS AT THE $g_{\|}$ EXTREME OF THE EPR LINE

BSD, bovine superoxide dismutase.

Sample	g [a] (MHz)	Frequency (MHz)	A_{zz} (MHz)	P_{zz} (MHz)
BSD-CN^-	2.445	17.7 ±0.3 19.3 ±0.4	37.0±1.3	≪1.6
		21.51±0.1 23.09±0.09	47.8±0.4	1.62±0.01
		24.55±0.07 26.53±0.12		
BSD-N_3^-	2.47	16.60±0.4 18.20±0.2	37.9±1	1.54±0.02
		19.60±0.2 21.36±0.35		
BSD [b]	2.42	17.7 ±0.3 19.3 ±0.2 21.1 ±0.4	38.7±1	0.86±0.01

[a] g-value at which ENDOR was performed.

[b] The assignment of these values is tentative because of anisotropy and possible inequivalence of the first shell nitrogens.

CN and N_3 derivative are given in Table I. One notices that the indicated pair splittings are close to what is expected for ^{14}N. The discrepancy for the high-frequency pair in the cyano complex (e.g., 1.98 vs. 1.64 MHz) probably comes about because of our use of a Hamiltonian that is accurate only to first order in the hyperfine constant. That is, the Hamiltonian (1) should also include the neglected terms,

$$A_{xx}S_X I_X + A_{yy}S_Y I_Y \qquad (3)$$

where A_{xx} and A_{yy} represent components of the hyperfine tensor along directions normal to the $g_{\|}$ direction. Because S_X and S_Y connect the two electronic $M = \pm 1/2$ manifolds, we know from second-order perturbation theory that the effect of expression 3 on the transition frequencies will be to modify them by no more than $\pm(A^2/2\nu_e)$, where $\nu_e = 9056$ MHz represents the microwave frequency. If we now associate $A_{xx} = A_{yy} = A(g_\perp)$ $= 55$ MHz (see Results section) and perform the perturbation calculation, we find that the predicted splittings increases to 1.97 MHz for only one pair. And this will be the high-frequency pair, provided that A_{zz} and P_{zz} have the same sign.

The second-order effect offers additional reason to accept the interpretation that the four-line pattern forms a cohesive unit corresponding to one type of strongly bound nitrogen. The situation is not as clear for the spectral feature centered at 18.5 MHz (Fig. 2). Here we have only a partially resolved resonance. Although it appears to be a nuclear Zeeman splitting characteristic of ^{14}N, there is no discernable quadrupole structure to give one confidence in the identification. One can, however, arrive at its identification as a nitrogen resonance by elimination of the other possibilities. The only candidates are those magnetic nuclei in or associated with the protein: i.e., zinc, copper, cyanide nitrogen, protons and protein nitrogen. The zinc (^{67}Zn) is an unlikely candidate because it is located several angstrons away from the major electronic spin density, its nuclear spin is 5/2 (implying up to eight ENDOR lines), and its nuclear magnetic moment is less than that of ^{14}N. The effect of the copper is ruled out because the ENDOR is performed at $g_{\|}$ where the ^{65}Cu hyperfine interaction is so large (≈ 200 G) that it shows up in the EPR spectrum itself. The resonance cannot be due to the cyanide nitrogen because the spectrum is unchanged when $C^{14}N$ or $C^{15}N$ is used. That it comes from a proton is ruled out by performing the ENDOR experiment at two different microwave frequencies (Fig. 2) while keeping the experimental g-value constant [21]. The nuclear Zeeman interaction for a proton is about 14-times larger than for a nitrogen. Since the interaction is proportional to the static field, we should see weakly coupled proton resonances centered about the free proton frequency, which itself will shift in proportion to the microwave frequency shift. On the other hand, a strongly coupled nitrogen's resonant position will be centered around $A/2$ (the dominant term) for both microwave frequencies. This experiment was described earlier (Results section), and the result in Fig. 2 shows the expected proton shift nearby the region of the free proton frequency (11 MHz). Because the resonance at 18.5 MHz does not show a similar shift, we identify it with a nitrogen belonging to the protein. Its lack of quadrupole structure implies, according to Eqn. 2, that $P_{zz} << 1.5$ MHz or perhaps that the quadrupole principal axis is not along H_0. A lack of structure in a strongly coupled nitrogen has been seen previously. For instance, the near nitrogen of the model compound tetraimidazole-Cu(II) [17] displayed a nitrogen ENDOR resonance devoid of structure and with a suspected small quadrupole effect. The proteins cytochrome c oxidase [23] and stellacyanin [21] also seem to have poorly resolved quadrupole structure in their nitrogen ENDOR spectra. The poor resolution from the model compound was thought to be the result of inequivalence either among the four near neighbor nitrogens or among molecular complexes.

A final test of our identification of the nitrogens in the 10 to 30 MHz region is possible because the EPR of the $+3/2$ (low-field) Cu(II) hyperfine peak in the cyanide derivative is resolved into seven lines. Taking the hyperfine constants 47.77 MHz and 37.1 MHz identified by ENDOR (15.48 G and 12.02 G for $g_{\|} = 2.208$), we can reconstruct a series of EPR simulations using the various permutations possible for three nitrogens. (We can only deal with three nitrogens because four would require nine peaks in the $+3/2$

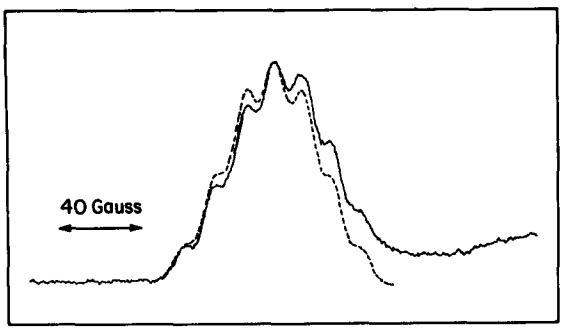

Fig. 9. Comparison of the experimental EPR spectrum (solid line) of the low-field ^{65}Cu hyperfine peak with a simulated EPR spectrum (dashed line) using two nitrogens with hyperfine coupling of $A = 47.77$ MHz (15.48 G for $g = 2.208$), and one nitrogen with coupling $A = 37.1$ MHz (12.02 G). The simulation used a gaussian lineshape with intrinsic linewidth of 12 G at half-height.

Cu(II) line). Fig. 9 shows the result for the best combination: two nitrogens with $A = 47.77$ MHz and one with $A = 37.$ MHz. Thus we have found that, of the three nearly equivalent nitrogens previously reported [4,8] only two are equivalent as determined by both ENDOR and EPR.

We note that similar simulations may be performed for the native and azido forms of the protein. For azide, four equivalent nitrogens having $A = 37.9$ MHz (12.1 gauss at $g = 2.24$) and an

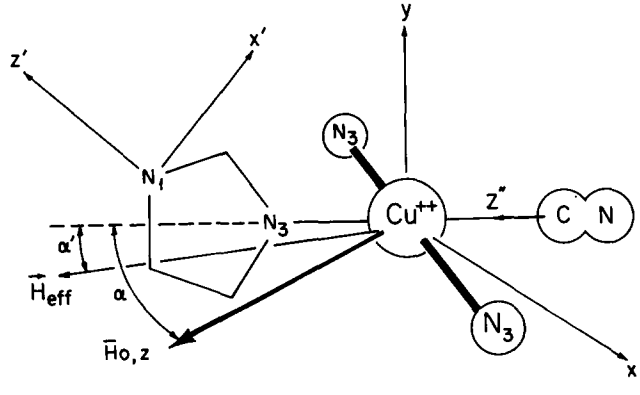

Fig. 10. A model for CN^- binding in bovine superoxide dismutase-CN^-. The nitrogens bonded to the copper via bold lines are magnetically equivalent. Also shown is the geometry used for the ENDOR simulations. A planar structure is formed by the copper, the three neighbor nitrogens, and the cyanide. The $g_{\|}$ direction is normal to this plane. The external field, $\vec{H}_0$, and the effective field, $\vec{H}_{eff}$, are shown at orientations that will contribute to simulated spectra at the $g_{\perp}$ extreme. The primed coordinates correspond to the principle axes of the quadrupole interactions of the outer shell nitrogens.

intrinsic linewidth of 15 G will yield a poorly resolved EPR lineshape having an overall half-width at half-eight of 52 G. The simulation agrees favorably with the experimental linewidth (≈ 53 G) and lineshape. The same procedure applied to the native protein yields a linewidth of 53 G, a value markedly less than the measurement (59 G). It seems that there exists more magnetic inequivalence in the native form than in the cyano and azido forms.

The results for the first shell nitrogens suggests a simple model for the cyano complex. We recall that two near neighbor nitrogens seem to be in magnetically equivalent environments that are qualitatively different from that of a third near nitrogen, characterized by its weaker hyperfine interaction. We may suppose that its bonding to the copper is somewhat different from that of the other two N-atoms. *Trans* influences have been described [24] in many substances whereby the bonding of a ligand to a metal ion is weakened by the presence of a stronger ligand opposite it. Taking the cyanide to be the stronger ligand, this suggests that, of the several copper ligands, the two equivalent nitrogens are symmetrically disposed relative to the CN^- and the third visible nitrogen. The simple model is illustrated schematically in Fig. 10. Here the cyanide is bound via the carbon and opposite the more weakly interacting nitrogen. The boldness of the bond is a schematic representation of the relative strengths of the nitrogen hyperfine interactions. The assumed direction of $g_{\|}$ is indicated by the vertical arrow near the Cu(II). One of three histidine imidazoles is drawn in the figure, but one should not infer the orientation of its plane from this discussion.

Low-frequency ENDOR

Because it consists of overlapping contributions from more than one distinct type of nucleus, the low-frequency region (1–10 MHz) is considerably more difficult to interpret than the high-frequency region. We know of these diverse contributions for two reasons: first, from ESE [14] and ENDOR [17] work on tetraimidazole-Cu(II) we have seen that the remote imidazole nitrogen spectrum has detectable intensity in the 1–4 MHz range, and second, the difference between the experimental $C^{14}N$ and $C^{15}N$ ENDOR spectra of the protein

convinces us that the cyanide nitrogen can also be observed in this frequency range. A single trace of this region with only one isotope present would provide little chance for interpretation in terms of a model for the complex. But we are fortunate to have four traces, two at the $g_{\|}$ extreme and two at the $g_{\perp}$ extreme (one trace for each isotope). We can add a fifth trace, in a sense, because, from the ESE of $C^{15}N$ [14], we are given a plot that is similar to ENDOR (i.e., the Fourier transform of the ESE envelope), but which furnishes additional information on the environment of the remote nitrogen. These five separate but related traces are sufficiently different to motivate a search for one self-consistent interpretation. Further motivation comes from the favorable computer simulations of the low-frequency region of tetraimidazole-Cu(II) published earlier [17] and duplicated in Fig. 8.

In what follows, the steric model for the Cu-CN complex, presented in the high-frequency section, will be used to interpret the low-frequency ENDOR. A nuclear Hamiltonian will be introduced and discussed. A somewhat qualitative discussion of the simplest of our cases, the $C^{15}N$-derivative spectra, will follow in order to find a starting point for analysis. A detailed discussion of the ENDOR powder pattern generation will follow with emphasis on the spectra taken at the $g_{\perp}$ extreme. The simulation method will then be applied to the imidazole remote nitrogen and compared to the ESE results [14]. Finally, composite (imidazole + CN) simulations of the $C^{15}N$ complex at $g_{\|}$, $g_{\perp}$, and $C^{14}N$ at $g_{\perp}$, $g_{\|}$ will be presented, in that order.

Our approach will be to proceed from the easiest to the most difficult to interpret of the traces and thereby obtain estimates of some parameters independently of the others. We note that a least-squares search is not really useful in this situation because there is no complete attempt to handle the ENDOR intensities. Despite that weakness, the major features of all the low-frequency spectra will be presented, using the steric model and one set of Hamiltonian parameters. Whether the model is unique will be briefly treated at the discussion's end.

The Hamiltonian. In order to relate the model to the low-frequency results, one must choose a form for the nuclear Hamiltonian that is capable of describing the components of all four experimental traces (four remote nitrogen atoms, two isotopes, two g-values). It will include hyperfine and quadrupole terms, but because two types of orientation for the complex are being considered, the possibility that these interactions are anisotropic must be included. For an unpaired electron spin, S, interacting with a nucleus with spin $I > 1/2$, we may write,

$$\mathcal{H}_N = \vec{S} \cdot \underset{\sim}{A} \cdot \vec{I} \pm g_N \beta_N \vec{H}_0 \cdot \vec{I} + Q_{z'z'}\left(3I_{z'}^2 - I(I+1)\right) + Q_{x'x'y'y'}\left(I_{x'}^2 - I_{y'}^2\right) \quad (4)$$

where the hyperfine interaction now is explicity written as being anisotropic, the nuclear Zeeman term is allowed to be $\pm$ depending on the sign of the magnetic moment of the respective nuclear iostope (>0 for ^{14}N, <0 for ^{15}N), and where the quadrupole terms are written in terms of their principal components, $Q_{z'z'}$, and the asymmetry term $Q_{x'x'y'y'}$. The quadrupole terms are only needed for ^{14}N since a spin $1/2$ nucleus (i.e., ^{15}N) has no quadrupole moment. The primes refer to the separate principal axis system for the quadrupole terms. For example, the (x', y', z') system for the imidazole's remote nitrogen [25] is shown by the dotted lines in Fig. 10. Lacking other information, we are assuming that the (x', y', z') system is the same as was found for the model compound tetraimidazole-Cu(II). The molecular reference frame, (x, y, z), in which S_z is diagonal and which defines the orientation of the static and effective magnetic fields, is also shown in Fig. 10. The static magnetic field will always be assumed to lie along one of the principal directions of the axial g-tensor.

A qualitative estimate. Of the five separate traces mentioned above, the one for bovine superoxide dismutase-$C^{15}N$ at the $g_{\|}$ extreme (Fig. 6) appears to be the easiest to interpret. At this field position, the unique relationship between $\vec{H}_0$ and the molecular coordinates should result in crystal-like ENDOR spectra similar to what we saw in the high-frequency region. Because the ENDOR at $g_{\|}$ from the remote nitrogen in tetraimidazole-Cu(II) was not easily observed, the rather strong peaks at 1.73 and 3.75 MHz (Fig. 6) are tentatively assigned to the $C^{15}N$. In this case, only the first two terms in

Eqn. 4 are needed. If we refer to $A_{\parallel}^{N}$ and $A_{\perp}^{N}$ as being the components of $\tilde{A}^{N}$ parallel to and perpendicular to the CN bond axis (note change in coordinate frame), then Eqn. 4 leads to this simple form for the ENDOR frequencies at $g_{\parallel}$,

$$\nu_{ENDOR} = \frac{A_{\perp}^{N}}{2} \pm g_N \beta_N H_0 \qquad (5)$$

For $H = 2475$ G, we expect $2 g_N \beta_N H_0 (^{15}N) = 2.14$ MHz. Considering that the linewidth (Fig. 6) is about 1 MHz, this is close enough to the measured separation of 2.02 MHz that one can infer a value of $A_{\perp}^{N} = 5.48$ MHz.

A more complicated spectrum is presented by the $C^{15}N$ derivative at the $g_{\perp}$ extreme. Because the field, $\vec{H}_0$, will lie in the plane of the complex, both $A_{\parallel}^{N}$ and $A_{\perp}^{N}$ will enter into determination of the ENDOR frequencies. The response of the remote imidazole nitrogens must also be taken into account because it is known to be detectable at this field position. The similarity between Figs. 4 and 8 together with the estimate that $\frac{A_{\perp}^{N}}{2} \cong 2.7$ MHz for $C^{15}N$ suggests that $A_{\parallel}^{N} > A_{\perp}^{N}$ and that $A_{\parallel}^{N}$ is responsible for the high-frequency tail above 4 MHz in Fig. 4. To support this conclusion, the composite ENDOR simulations for the imidazole's remote nitrogen and the cyanide nitrogen will be computed.

Powder pattern generation. We consider the Hamiltonian in Eqn. 4 as the starting point for the ENDOR simulation of the bovine superoxide dismutase-CN complex as shown in Fig. 10. Here we are especially concerned with the $g_{\perp}$ extreme; the static magnetic field then lies in the plane of the complex (i.e., the x, z plane in the figure). Before energy levels and transition frequencies can be found from Eqn. 4 the various terms must be expressed relative to the same reference frame. From the high-field approximation we take the electron spin to be quantized along the direction of the external magnetic field, $\vec{H}_0$, and the nuclear spin to be quantized along the resultant of $\vec{H}_0$ and the hyperfine field, i.e., the effective field, $\vec{H}_{eff}$. For $C^{15}N$, the energy levels will then be given by $E = g_N \beta_N |H_{eff}| m$, where $m (= \pm 1/2)$ expresses the nuclear magnetic quantization and,

$$|H_{eff}| = \frac{H_0}{\nu_0} \left[\left[M_S A_{xz} \right]^2 + \left[\nu_0 - M_S A_{zz} \right]^2 \right]^{1/2} \qquad (6)$$

Here $\nu_0 = g_N \beta_N H_0$, $M_S = \pm 1/2$, and A_{xz} and A_{zz} are components of the hyperfine tensor expressed in the (x, y, z) system of the external field, i.e.

$$A_{xz} = \left(A_{\parallel}^{N} - A_{\perp}^{N} \right) \sin\alpha \cos\alpha$$

$$A_{zz} = A_{\parallel}^{N} \cos^2\alpha + A_{\perp}^{N} \sin^2\alpha \qquad (7)$$

The angle α specifies the direction of the external field relative to the CN-Cu-N axis.

To obtain the energies for the bovine superoxide dismutase-$C^{14}N$ case we repeat the above procedure, but now must include the quadrupole terms. We let (x', y', z') and (x'', y'', z'') refer to the directions of the principle axes of the remote imidazole and $C^{14}N$ nitrogens, respectively. Some of these directions are shown in Fig. 10 with the choice for z'' being justified later. Since the quadrupole Hamiltonian is expressed in terms of the nuclear spin alone, we need only to transform it to the reference system for which the nuclear spin is approximately diagonal; this is the effective field system again. Because the hyperfine interaction of the cyanide nitrogen is anisotropic, however, the effective field will not in general be colinear with the external field. We represent this different angle by α' in Fig. 10; the components of $\vec{H}_{eff}$ can be used to find α' (note that $\alpha' = \alpha$ for an isotropic hyperfine interaction). If the largest term in the cyanide quadrupole interaction is transformed to the reference frame of the effective field, it becomes,

$$3Q_{z''z''} \left(I_x^2 \sin^2\alpha' + I_z^2 \cos^2\alpha' - \{I_x, I_z\} \cos\alpha' \sin\alpha' - 2/3 \right) \qquad (8)$$

where $\{I_x, I_z\} = (I_x I_z + I_z I_x)$. We will show later that the asymmetry term is negligible for interpretations of our bovine superoxide dismutase-CN spectra.

In order to obtain the frequencies contributing to the powder pattern, we proceeded as follows. The orientation of $\vec{H}_0$, as given by α, was varied incrementally. At each interval, the transition energies that proceed from Eqns. 4 through 8 were calculated for $M = \pm 1/2$ using direct diagonalization of the secular matrix derived from the quadrupole interaction. The intensities of transitions were taken to be unity; they were then

modified only with respect to the ENDOR enhancement effect [26,27] in a way suggested for anisotropic hyperfine interactions by Atherton [28]. Finally, a histogram in frequency space was built up with a resolution of approx. 0.032 MHz (i.e., 250 points per 8 MHz), and this was convoluted with a lineshape followed by normalization to the experimental spectrum. The calculations were performed using a Bruker Aspect-2000A minicomputer.

Simulations

Imidazole. The low-frequency ENDOR experiment described here is sensitive to the broad features of the imidazole spectrum [17], and these are mixed with the cyanide spectrum. The ESE experiment, on the other hand, is sensitive to some sharp features in the imidazole's quadrupole structure not seen by us [17], but it is insensitive to any broad shape in the cyanide EPR spectrum [30]. For this reason, it is to our advantage to try first to simulate the ESE result for the $C^{15}N$-derivative [14].

Whether the ESE result is indicative of only one type of remote nitrogen is relevant to this work. The near nitrogen ENDOR has implied that there are at least two types of histidine bound to the copper. From this one may wonder whether there are at least two types of remote nitrogen. Further, evidence that the Zn-His-Cu bridge has not been broken [14] when cyanide is bound allows for the possibility of three inequivalent remote nitrogens. Nevertheless, we shall assume the simplest case of only one type of remote nitrogen.

In Table II we present the parameters used for the approximate recreation of the ESE result [14] for the imidazole only. This re-creation refers not to the simulation of the Fourier transform of the ESE envelope, but rather to a simulation of the ENDOR with all ENDOR enhancement effects removed. Whereas ESE observed sharp lines at 0.55, 0.8 and 1.35 MHz plus a broad peak at 3.5 MHz, our simulation yields sharp frequencies at 0.5, 0.9 and 1.4 MHz plus one at 3.74 that is not particularly broad. Given our simplification and available resolution, the comparison seemed satisfactorily. The parameters in Table II are not greatly different from the ones arrived at for tetraimidazole-Cu(II). At least, they are not significantly different at the resolution available in our experiment at $g_\perp$. Using these parameters, the ENDOR simulation of the remote nitrogen would resemble Fig. 8.

$C^{15}N$ at $g_\parallel$. The composite simulation in this case will test the earlier conjecture (see Qualitative estimate) that the two peaks in Fig. 4 are primarily due to the $C^{15}N$. The dashed line in Fig. 6 shows the contribution from three remote nitrogens plus one $C^{15}N$. It has turned out that the two simulated spectra overlap here also. Although we have observed that the remote nitrogen ENDOR response was weak at $g_\parallel$, the simulated trace corresponds to a substantial contribution from it in the peak at the lower frequency, but the dominant contribution to the peak at the higher (3.75 MHz) frequency is from $C^{15}N$. The relatively greater intensity of the $C^{15}N$ (even though it is only one molecule versus three imidazoles) comes from there being half as many transitions among which to distribute intensity (i.e., $I = 1/2$ vs. $I = 1$), and from its

TABLE II

PARAMETERS USED IN SIMULATION FOR BOVINE SUPEROXIDE DISMUTASE-CN

		Remote IM-^{14}N (MHz)	$C^{14}N$ (MHz)	$C^{15}N$ (MHz)
	$A_\parallel^N$	1.6	5.7	8.0
	$A_\perp^N$	1.6	3.9±0.3	5.47±0.4
	$Q_{z'z'}$	0.376	1.0±0.1	—
	$Q_{x'x'y'y'}$	0.25	0	—
$g_N\beta_N H_0$	at $g_\parallel$	0.77	0.77	1.075
	at $g_\perp$	0.98	0.98	1.36

having a larger hyperfine constant. That is, ENDOR intensity increases roughly as the square of the ratio of the hyperfine constant to the nuclear Zeeman energy [28]. The $g_{\|}$ simulation required the intrinsic linewidth for convolution to be 0.8 MHz. Since this simulation was the simplest of the four ENDOR traces, we used its value of intrinsic linewidth for the following three simulations as well.

$C^{15}N$ at $g_{\perp}$. Here, both $A_{\|}^{N}$ and $A_{\perp}^{N}$ contribute to a powder pattern that consists of two envelopes. Using Eqns. 6 and 7 with $\alpha = 0°$ and 90°, one finds that the envelopes will be separated by $2g_N\beta_N H_0$ and will have upper and lower limits determined by $(A_{\|}^{N}/2$ or $A_{\perp}^{N}/2) \pm g_N\beta_N H_0$. At this point one can take $A_{\perp}^{N}$ to be known from Eqn. 5 and adjust $A_{\|}^{N}$ until it contributes to the tail at 5–6 MHz in Fig. 4. The highest frequency that could contribute is $A_{\|}^{N}/2 + g_N\beta_N H_0$. At $g = 1.955$, the values of the nuclear Zeeman term is 1.36 MHz. So a value of $A_{\|}^{N} = 8.0$ MHz was chosen. The combined powder pattern is given by the dashed line in the middle of Fig. 4. The enhancement effect turns out to be less critical for the cyanide nitrogen's simulated ENDOR lineshape than for the imidazole's remote nitrogen lineshape [17]. That is, the ratio of contributions to the intensity from the $M = \pm 1/2$ manifolds was about 5 : 1 for the cyanide, but was about 3000 : 1 for the remote nitrogen [17]. Both types of nitrogen contribute to the feature near 2 MHz, with the dominant contribution coming from the imidazole. The cyanide nitrogen dominates in the region beyond 4 MHz.

We note that neither the ENDOR simulation nor the ENDOR experiment predicts [17,30] the observed ESE result for the $C^{15}N$ derivative [14]. The sharp lines present in the ESE Fourier transformed envelope are easily reconciled to our result using the ENDOR enhancement effect, but the discrepancy between the positions of the higher frequency peaks is not well understood. (The ESE result shows a broadened somewhat symmetric peak near 3.5 MHz, but the ENDOR experiment (and simulation) shows an asymmetric feature near 4 MHz.) The origin of this small discrepancy is not presently understood.

$C^{14}N$ at $g_{\perp}$. The only change here is to substitute ^{14}N for ^{15}N in the cyanide and try to duplicate the observed spectral changes. There is no need to search for new values for the hyperfine constants since they are proportional to the ratio of the magnetic moments (i.e., the ratio of the ^{14}N magnetic moment to that of ^{15}N is 0.713). So for $C^{14}N$, one sets $A_{\|}^{N} = 5.71$ MHz and $A_{\perp}^{N} = 3.91$ MHz. With the introduction of $C^{14}N$, one must also introduce the quadrupole effects. In principle, these effects require for new variables, two constants ($Q_{z''}$ and $Q_{x''x''y''y''}$), and two principal directions (z'', x''). Rather than perform a grid search over these variables, we referred to the work of Ikeda et al. [29], who have done pure quadrupole resonance on a host of metal cyano complexes including Zn(II), Cd(II), Hg(II) and Cu(I). For these metals, they found that $3Q_{z''z''}$ (their ν_0) $\cong$ 3 MHz, $Q_{x''x''y''y''} = 1$–3% of $Q_{z''z''}$, and Z'' was along the CN bond direction. From these results we took some justification for setting $Q_{x''x''y''y''} = 0$ and thus reduced the number of new variables to two. Further, we simply set $Q_{z''z''} = 1$ MHz with the z'' direction along the CN direction. The simulation is given by the dashed line in the middle of Fig. 5. In order to see the effect of the cyanide more clearly here, we had to perform the simulation using a ratio of one imidazole to one cyanide. The low peak near 7 MHz provides a good measure of the strength of the quadrupole interaction. If the interaction varied by 10%, the position of the peak would shift by 0.3 MHz. The linewidth as seen in the lower trace of Fig. 5 is about 0.6 MHz. For this reason, $Q_{z''z''}$ for cyanide is given in Table II as 1 ± 0.1 MHz.

$C^{14}N$ at $g_{\|}$. Finally, having determined all constants, one can obtain a self-consistent check by comparing a simulation of the $C^{14}N$-derivative to what is observed at the $g_{\|}$ extreme. Because this field position should yield crystal-like ENDOR spectra, the experimental spectrum would have been valuable. Unfortunately, the observed spectrum has poor S/N and so has been used only as a final check. The dashed line on Fig. 7 shows the simultion for three imidazoles plus one cyanide. The intensities are weaker than in Fig. 6 (as expected), since the $C^{14}N$ spectrum is spread out by the quadrupole interaction. Despite the poor S/N of the experimental trace, there does not appear to be any gross inconsistency.

Final remarks

The foregoing simulations have several weak points. The ENDOR intensities, for instance, were not handled in an entirely realistic way. That is, we have included no details of an ENDOR mechanism as it may apply to the intrinsic transition probability; nor have we included any effects due to rapid passage. Both of these effects may have influenced our need to use a 1:1 ratio of imidazole to cyanide in Fig. 5 rather than 3:1 as in the other cases. It was pointed out too that the passage conditions affect the details of the lineshape. In addition, our assumption of equivalent remote imidazole nitrogens is probably wrong. At the present resolution, however, we have supposed that the effect of inequivalence either is too small to notice or is difficult to disentangle from the cyanide spectrum. Because it seemed impractical, the uniqueness of the steric model was not fully explored. The only other model for the cyano complex investigated in this study placed the cyanide along the axial ($g_{\|}$) direction. Although this configuration was capable of yielding satisfactory simulations at the $g_{\|}$ extreme, it did not yield satisfactory powder patterns at the $g_{\perp}$ extreme, and so it was discarded.

Despite the complicated low-frequency lineshape, our analysis does have some strong points worth summarizing. We did not have to resort solely to a grid search over the many parameters needed for an adequate description. Instead we could approach the final simulations step by step, making use of many independent results in a cohensive way. Among them were: (1) the ENDOR observations at two field positions using two isotopes of cyanide, (2) the previous ENDOR and ESE studies of the model compounds, (3) the ESE observations of bovine superoxide dismutase-$C^{15}N$, (4) the pure quadrupole resonance results on cyano-metallic compounds, and (5) the new information found for the strongly coupled nitrogens in bovine superoxide dismutase-CN. The equiplanar binding scheme appears to be a simple way of correlating all the above observations.

Conclusions

The copper (II) site in the native, azido and cyano form of bovine superoxide dismutase has been examined using the ENDOR technique. Electron-nuclear hyperfine and nuclear quadrupole interactions associated with the directly coordinated nitrogens have been observed in each case. Moreover, the interactions associated with the remote nitrogens of the imidazole and cyanide have been observed for the cyano derivative. The ENDOR response of the native form was not readily interpreted, but it did suggest an inequivalence with respect to the hyperfine interaction of the near neighbor nitrogens. The response of the azido form, however, suggested that four nearly equivalent nitrogens surrounded the copper, their hyperfine interaction being not quite large enough to show up in the EPR lineshape at $g_{\|}$. The response of the cyano form of the protein was the most informative. Of the three EPR-observable nitrogens, two are magnetically equivalent and have hyperfine and quadrupole intractions that are larger than the third nitrogen. The three nitrogens, the copper and the cyanide are envisioned to form a plane so that the cyanide is *trans* to the more weakly coupled nitrogen.

The attainment of this configuration around the Cu(II) without breaking and protonating the imidazolate bridge [14,31] requires displacement of either His-44, -46 or -118 from the Cu(II). The extremely low NMR relaxivity of the monocyano derivative [8] suggests that water molecules cannot bind directly to the Cu(II), thus implying that the displaced histidine is coordinated as an axial ligand. This model is consistent with, but not proven by, these spectral observations.

Acknowledgements

We wish to thank W.B. Mims and J. Peisach for making available pre-published ESE results. We also thank W.E. Downer and W.R. Dunham for help in the construction of the apparatus. This work was supported by an NIH Postdoctoral Service Award (to H.V.C.) AM 05588, and United States Public Health Service Research Grants GM 12176 (to R.H.S.) and GM 21519 (to J.A.F.).

References

1 Richardson, J.S., Thomas, K.A. and Richardson, D.C. (1975) Biochem. Biophys. Res. Commun. 63, 986–992

2 Richardson, J.S., Thomas, K.A., Rubin, B.H. and Richardson, D.C. (1975) Proc. Natl. Acad. Sci. U.S.A. 72, 1349–1353
3 Tainer, J.A., Getzoff, E.D., Beem, K.M., Richardson, J.S. and Richardson, D.C. (1982) J. Biol. Chem., submitted for publication
4 Fee, J.A. (1981) in Metal Ions in Biological Systems (Sigel, H., ed.), vol. 13, pp. 259–298, Marcel Dekker, New York
5 Rigo, A., Stevanato, R., Viglino, P. and Rotilio, G. (1977) Biochem. Biophys. Res. Commun. 79, 776–783
6 Gaber, B.P., Brown, R.D., Koenig, S.H. and Fee, J.A. (1972) Biochem. Biophys. Res. Commun. 57, 845–848
7 Fee, J.A. and Gaber, B.P. (1972) J. Biol. Chem. 247, 60–65
8 Rotilio, G., Morpurgo, L., Giovagnoli, C., Calabrese, L. and Mondovi, B. (1972) Biochemistry 11, 2187–2192
9 Fee, J.A. (1973) Biochem. Biophys. Acta 295, 107–116
10 Beem, K.M., Rich, W.E. and Rajagopalan, K.V. (1974) J. Biol. Chem. 249, 7298–7305
11 Rotilio, G., Finazzi-Agro, A., Calabrese, L., Bossa, F., Guerrieri, P. and Mondovi, B. (1971) Biochemistry 10, 616–621
12 Haffner, P.H. and Coleman, J.E. (1973) J. Biol. Chem. 248, 6626–6629
13 Lieberman, R.A., Sands, R.H. and Fee, J.A. (1982) J. Biol. Chem. 257, 336–344
14 Fee, J.A., Peisach, J. and Mims, W.B. (1981) J. Biol. Chem. 256, 1910–1914
15 McCord, J.M. and Fridovich, I. (1969) J. Biol. Chem. 244, 6049–6055
16 Fee, J.A. (1973) J. Biol. Chem. 248, 4229–4234
17 Van Camp, H.L., Sands, R.H. and Fee, J.A. (1981) J. Chem. Phys. 75, 2098–3007
18 Van Camp, H.L., Scholes, C.P. and Isaacson, R.A. (1976) Rev. Sci. Instrum., 47, 516–517
19 Dorio, M.M. and Freed, J.H. (eds.) (1979) Multiple Electron Resonance Spectroscopy, Plenum, New York
20 Rist, G.H. and Hyde, J.S. (1968) J. Chem. Phys. 49, 2449–2451
21 Rist, G.H., Hyde, J.S. and Vanngård, T. (1970) Proc. Natl. Acad. Sci. U.S.A. 67, 79
22 Van Camp, H.L., Scholes, C.P., Mulks, C.F. and Caughey, W.S. (1977) J. Am. Chem. Soc. 99, 8283–8290
23 Van Camp, H.L., Wei, Y.H., Scholes, C.P. and King, T.E. (1978) Biochem. Biophys. Acta 537, 238–246
24 Appleton, T.G., Clark, H.C. and Manzer, L.E. (1973) Coord. Chem. Rev. 10, 335–422
25 Ashby, C.I.H., Cheng, C.P. and Brown, T.L. (1978) J. Am. Chem. Soc. 100, 6057–6063
26 Davies, E.R. and Reddy, T.R. (1970) Phys. Lett. 31A, 398–399
27 Whiffen, D.H. (1968) Mol. Phys. 10, 595–596
28 Atherton, N.M. (1973) Electron Spin Resonance, pp. 367–376, John Wiley, New York
29 Ikeda, R., Nakamura, D. and Kubo, M. (1968) J. Phys. Chem. 72, 2982–2986
30 Mims, W.B. and Peisach, J. (1978) J. Chem. Phys. 69, 4921–4930
31 Calabrese, L., Cocco, D., Morpurgo, L., Mondovi, B. and Rotilio, G. (1976) Eur. J. Biochem. 64, 465–470